Heat Transfer Engineering, 26(3):89–98, 2005
Copyright © Taylor & Francis Inc.
ISSN: 0145-7632 print / 1521-0537 online
DOI: 10.1080/01457630590907419

Taylor & Francis
Taylor & Francis Group

Direct Comparison between Five Different Microchannels, Part 2: Experimental Description and Flow Friction Measurement

CORMAC EASON, TARA DALTON, and MARK DAVIES
Stokes Research Institute, University of Limerick, Co. Limerick, Ireland

CIAN O'MATHÚNA and ORLA SLATTERY
NMRC, University College Cork, Cork, Ireland

Part one of this paper [1] investigates the manufacture of five types of microchannels produced by wet and dry etching in silicon and precision mechanical sawing in silicon and thermoset plastic. This paper describes the experimental equipment and methods used to measure the pressure flow characteristics of the manufactured channels. A test system has been built to test each sample using the same inlet and outlet manifolds, pressure tappings, pumping system, and instrumentation. The measured pressure flow behavior was compared with theoretical values calculated from macroscale theory. Error analysis was carried out in order to determine the overall accuracy of the experimental work and determine the significance of any experimental deviation from theoretical values. An area compensation term is introduced to account for the difference in cross-section between the measured actual channels and the rectangles/trapeziums that share their overall dimensions.

A considerable body of research has been performed on fluid flow in microchannels with inconclusive results. Variation in measured friction factors from 0.5–2.5 times the predicted theoretical values have been reported by six separate experimenters [2]; another study [3] references papers measuring friction factors above and below theoretical values but finds no experimentally significant deviation from expected values at all. Other research also reports experimental values close to theoretical predictions [4, 5]. This paper aims to produce reliable data to add to the body of information already available in the area of pressure drop through microchannels.

The manufacturing methods used were developed with the NMRC and made use of precision sawing in plastic, silicon, and glass; deep reactive ion etching (DRIE), and KOH etching. The manufacturing processes and measurement of the dimensions of the channels are detailed in part one of this paper [1].

Many thanks to Paddy O'Regan for his machining work on the custom designed parts of the test system.

Address correspondence to Cormac Eason, Stokes Research Institute, University of Limerick, Co. Limerick, Ireland. E-mail: ceason@skynet.ie

Fundamental to any study to be performed on microchannels is the equipment used to test them and measure their behavior. A system where the channels are covered by a glass slide and clamped in place to create a seal was designed in order to allow easy dismantling and cleaning of the system as well as providing visual access to the channels. This has the advantage that problems such as air bubbles, blockages, and other unexpected behavior can be seen without dismantling the system.

EXPERIMENTAL DESCRIPTION

The microchannel test apparatus comprises of a gear pump, a fluid reservoir, tubing to join the microchannel modular block to the pumps, and two micrometer adjustable needle valves to control flow to the microchannel array.

The reservoir has a diameter of 270 mm. The reason such a large diameter was chosen is to prevent significant changes in the liquid height over the duration of an experiment. In addition, the reservoir is covered to prevent contamination from the air from settling into the water.

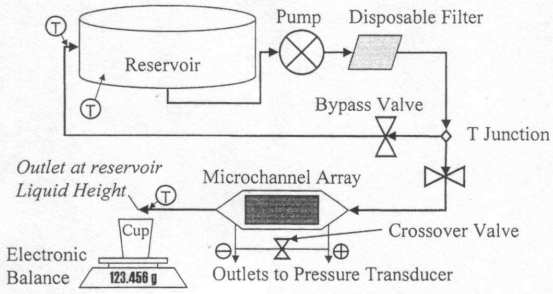

Figure 1 Schematic of the microchannel characterization equipment. The encircled Ts indicate where thermocouples are fitted to the system.

The pump motor is a feedback-controlled Tuthill V2DC unit that will deliver speeds from 60–3600 rpm. The motor is magnetically coupled to a Tuthill DDS.19 gear pump. This pump can supply pressures of up to 1.72 MPa at a temperature of 177°C. The pump supplies a flow rate of 0.19 ml/revolution, assuming zero slip in the pump. The liquid used for all tests described here is distilled and deionized water.

The micrometer adjustable valves have been named the *master* and *bypass* valves and are fitted as in Figure 1, with the master valve in series with the pump and channels and the bypass valve controlling flow through a tube that bypasses the microchannel block, returning directly to the reservoir. Using this system, steady flow rates much lower than those the pump delivers can be directly supplied to the channels. Closing the bypass valve diverts all flow through the channels.

K-Type thermocouple probes are used to measure the temperature of the reservoir, bypass circuit, and the temperature of the exiting fluid. The purpose of these thermocouples is to investigate whether there is any significant temperature change in the system over the course of the experiment. Viscous heating has been calculated to be negligible for the channels and flow rates tested; the pump, however, does add some heat to the system.

The pressure drop across the channels is measured using a Validyne DP15 differential pressure transducer. This transducer measures the change in inductance caused by the deflection of a diaphragm due to the pressure difference between its two sides. By using diaphragms of varying thicknesses, pressure ranges from a full scale of 860 ± 2 Pa to a full scale of 22,000 ± 55 MPa can be measured. For the experiments described here, a diaphragm with a pressure range from 0 to 14 kPa was used.

By adjusting the pump speed and valve settings, the system is capable of a supplying steady flow ranging from a maximum of 10.3 g/s to less than 0.015 g/s at pressures up to 1.72 Mpa. This mass flow range is beyond the capabilities of any in-line mass flow measurement device the authors are aware of. For this reason, weighing the fluid pumped through the system over a timed interval was the method used to take mass flow readings.

A digital balance and stopwatch are used for the mass and time measurements. All measurement durations apart from the maximum flow rates through the trapezoidal channels were at least sixty seconds. Measurements of evaporation from a collection cup over four days predict that approximately 1.4 mg of water will be lost over a minute. This is negligible compared to the ±1 drop (0.08 g) uncertainty already associated with the mass measurement. All mass measurements are of 3 g or more. The time over which the mass is collected is measured using a quartz stopwatch accurate to ±5 seconds/month. Operator error in the use of this device is taken to be ±0.5 seconds.

As shown in Figure 2, the fluid is sealed into the block by gasket paper (3) compressed by a glass slide (2), which is clamped in position by a cover plate (1). The 16 × 30 mm sample (4) fits into the shim (5), which then fits into a recess in the manifold block (6). Because the samples are available in a variety of thicknesses, several shims have been made with different depth grooves. The result of this is that all the channel samples, when fitted in their corresponding shims, occupy the same volume. Since the only change in the flow system from sample to sample is the size of the channels being tested, the effects of different manifolds, pressure tapping locations, and thermocouple locations as experienced in systems where each set of channels is machined with its own manifold are eliminated.

APPARATUS CALIBRATION

Prior to performing any experiments, the test system must be shown to produce repeatable data as well as steady flow. The steadiness of the gear pump motor was confirmed by using an optical digital tachometer to measure the actual pump speed in order that it could be compared to the speed indicated by the pump. All results from this test measured the pump speed to be accurate to less than ±1 rpm regardless of load or speed. This improves on the manufacturer's claim of ±9 rpm accuracy. Repeated flow tests at the same pump settings and different time intervals show the pump output to be steady.

The pressure transducer was calibrated using columns of water. The voltmeter is a digital auto-ranging model made by Fluke. It reads to 0.1 mV from 2 to 12 V and to 0.01 mV below 2 V. Because of the static nature of the loading on the transducer during calibration, readings were stable to ±0.5 mV. During experimental readings, the voltmeter is stable to ±50 mV (see Table 1). The overall error for pressure readings during the calibration of the transducer, accounting for errors in reading the water level, curve fitting error, and Voltmeter fluctuation, is ±42.5 Pa, or 0.3% of full-scale deflection.

The point data recorded during the calibration fit almost perfectly to a straight line through the origin (Correlation coefficient $r^2 = 0.999995$), allowing the slope of the best fit line to be confidently used to convert the voltage reading produced by the transducer to a pressure reading in Pascal. This constant, C = 871.98 Pa/V, and the curve and data points from which it is generated are shown in Figure 3.

K-Type thermocouples were used for all readings. They were calibrated in a temperature-controlled water bath to read

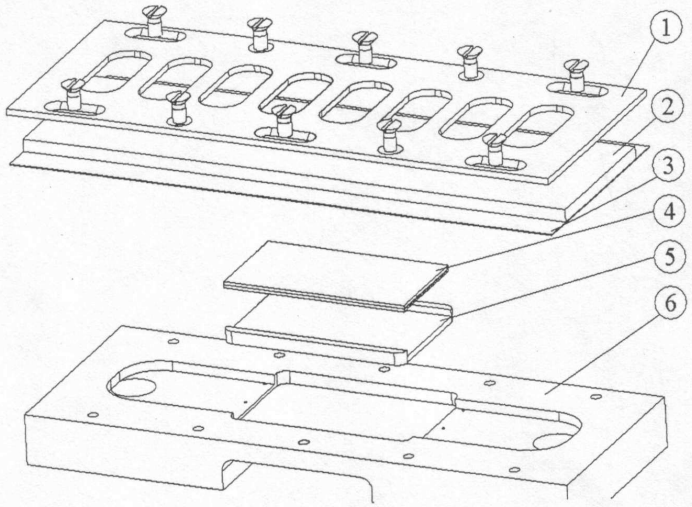

Figure 2 Layout of the microchannel tester.

accurately to ±0.1 K. The weighing scales used is a Sartorius BL150S digital balance, factory calibrated to ±0.001 g and able to measure masses of 150 g.

EXPERIMENTAL PROCEDURE

The experimental procedure begins with ensuring the apparatus is set up correctly. The electronic balance is leveled, and the outlet pipe from the microchannel test section is adjusted to the same height as the fluid in the reservoir. The reservoir height is indicated by a tube that siphons water from the reservoir and is held beside the outlet from the channels.

Once the initial set up is complete, the master valve is opened and the pump turned on at low speed. Opening the crossover valve between the positive and negative sides of the pressure transducer and running the pump at full speed remove any bubbles visible in the system. The crossover valve is opened to eliminate the possibility that the pressure transducer is overloaded.

To record a data point on the pressure flow curve, the pump speed and master/bypass valves are adjusted until a target pressure drop is indicated by the voltmeter. The system is left to settle for about a minute, and the scales are zeroed, and a timed mass flow reading begins. Each reading is repeated at least twice and usually three or more times for a given pressure setting. The flow through the system is then readjusted to give a new pressure drop, and the process is repeated again. At least two complete flow curves were recorded for each channel type.

Table 1 Experimental uncertainty. Values in bold indicate where the experimental uncertainty and the stated accuracy of a particular measurement differ

Measurement	Stated accuracy	Experimental uncertainty
Temperature	±0.1°C	±0.1°C
Voltage (Fluke voltmeter)	±0.0001 V	**±0.05 V**
Mass	±0.001 g	**±0.08 g**
Time	±0.01 s	**±0.5 s**
Master/bypass valves	±1/50th turn	±1/50th turn
Pump RPM	±9 rpm	**±1 rpm**

CALCULATIONS

The quantities listed in Table 2 are measured directly from the test system. A program written in Matlab was then used to convert this raw data into pressure and mass flow results. A second program calculates the theoretical pressure drop in the channels based on their shape and aspect ratio. Further work will allow the same program to predict the Nusselt number. The data used for these calculations was intended for large size channels and can be found elsewhere [6, 7]. The

Table 2 Raw data measured from the test system

Description	Symbol	Unit
Fluid temperature at bypass outlet	T_{bp}	°C
Fluid outlet temperature	T_o	°C
Reservoir temperature	T_{res}	°C
Bypass valve setting	V_{bp}	rev
Master valve setting	V_m	rev
Pressure transducer voltage	V_P	V
Mass of liquid flowing through system	M	g
Pump RPM	n	rev/min
Time taken for fluid to be collected	t	s

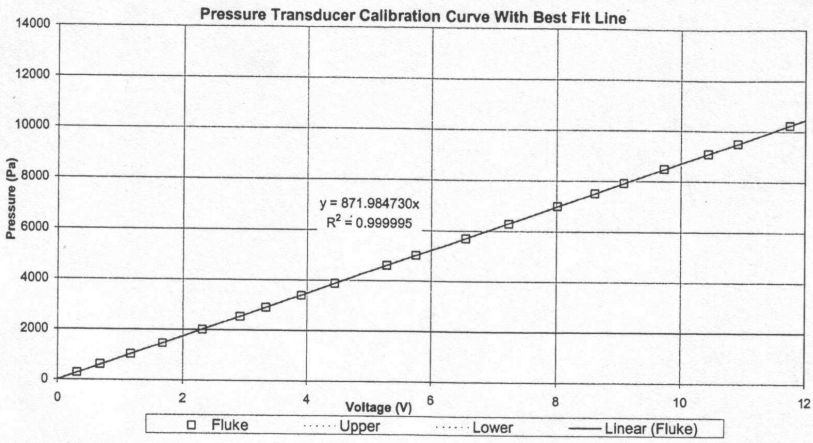

Figure 3 Calibration curve for pressure transducer with upper and lower uncertainty envelope. Note the correlation coefficient for best fit line is almost 1. A correlation coefficient of 1 means a perfect correlation.

channel dimensions are the averaged dimensions of the channels in each sample, as measured using a Scanning Electron Microscope (SEM) [1].

Because the pressure tappings do not coincide with the channel entrance and exit, the pressure drop measured by the experimental apparatus includes the contraction and expansion losses at the entrance and exit of the channels and the friction losses experienced by the fluid as it travels through the manifold from the pressure tappings to each end of the channels.

Darcy's Equation is used to calculate the pressure drop for fluid flowing in the channels and the inlet and outlet manifolds. Setting the friction factor f equal to 16/Re gives the correlation for laminar flow. It should be noted that when μ, ρ, and D_h remain constant, P_L is directly proportional to the mass flow rate $\dot{m}$ for laminar flow. Data measured from the system confirm this proportionality.

To account for the contraction and expansion losses at the entrance and exit of the channels, a similar equation is used [8]. This is shown in Eq. (1):

$$P_L = K_L \frac{\rho u^2}{2} \tag{1}$$

where P_L is proportional to $\dot{m}^2$. This is why the result plots are not perfectly linear. It should be noted that the contraction, expansion, and manifold friction losses form less than 8.7% of the total pressure drop for even the highest Reynolds numbers used here and are less than 1% at lower Re values. The value of K_L changes depending on the area ratio between the channel and the manifold. The manifold area divided by the number of channels in the sample is used as the $A1$ for the inlet and $A2$ for the outlet calculation. To calculate K_L for inlet loss, the Matlab program interpolates linearly between the values given in Table 3.

K_L for expansion losses is found using Eq. (2):

$$K_L = \left(1 - \frac{A1}{A2}\right)^2 \tag{2}$$

Once the program has been given the correct channel and manifold dimensions, it calculates the pressure drop, Reynolds number, Nusselt number, and friction factor for the channels. All these calculations are based on existing correlations for large channels.

UNCERTAINTY ANALYSIS

Table 1 shows a list of all the information recorded from the test system during each experiment, as well as the manufacturer's stated uncertainty for each measurement and the actual experimental uncertainty for each measurement as it performed in the experimental apparatus.

In order to calculate the experimental uncertainty in the mass flow, the formula in Eq. (3) was used [9].

$$w_{\dot{m}} = \left[\left(\frac{\partial \dot{m}}{\partial t} w_t\right)^2 + \left(\frac{\partial \dot{m}}{\partial m} w_m\right)^2\right]^{\frac{1}{2}} \tag{3}$$

This calculation is performed on every mass flow measurement. In order to produce a single mass flow figure to describe the accuracy of a flow curve, the uncertainty figures were averaged and their sample standard deviation found. A 95% confidence interval (CI) for the mass flow uncertainty is found by adding 1.65× the standard deviation to the average

Table 3 Loss coefficient vs. area contraction ratio [8]

$A2/A1$	0	0.1	0.2	0.4	0.6	0.8	0.9	1
K_L	0.5	0.37	0.35	0.27	0.17	0.06	0.02	0

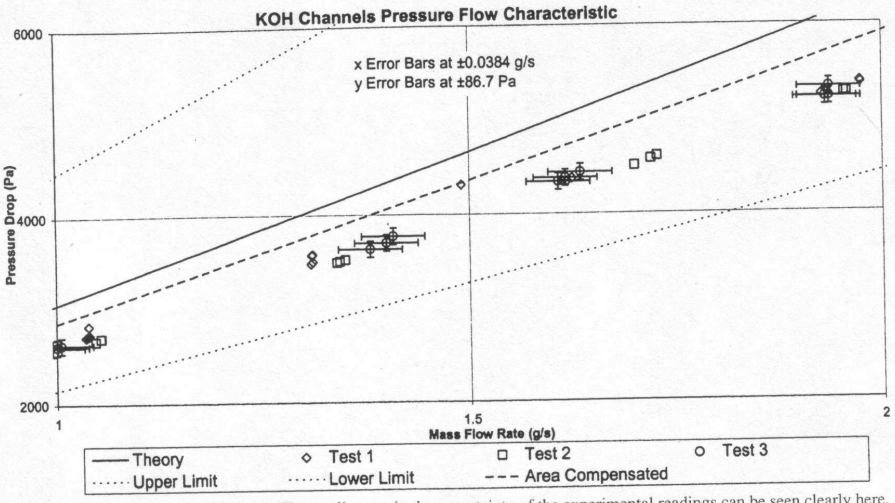

Figure 4 Zoomed area on Figure 9. The small range in the uncertainty of the experimental readings can be seen clearly here.

uncertainty. A standard 95% CI is the average value ±2 standard deviations, but since all the lower values of the uncertainty indicate greater than average accuracy, 95% of all results will be contained in the range from zero to the average plus 1.65 standard deviations. The calculated uncertainties are shown in error bars on the flow curves plotted in the results section.

Uncertainty in pressure measurement was calculated by adding the calibration error for the transducer (±42.5 Pa) to the extra uncertainty caused by the increase in fluctuation in the voltmeter as a result of performing measurements on a dynamic system. The resulting error is ±86.7 Pa, as is shown on the error bars in the result plots. It is a very small error in comparison with the pressures being measured (0.63% of Full Scale Deflection), so the y error bars can only be seen clearly in Figure 4.

RESULTS

Five different types of channels were tested (see Table 4). Detail on how the channels were measured can be seen in Part one of this paper [1].

DISCUSSION

It can be seen from the pressure flow curves in Figures 4 through 9 that all the curves except for those recorded for the

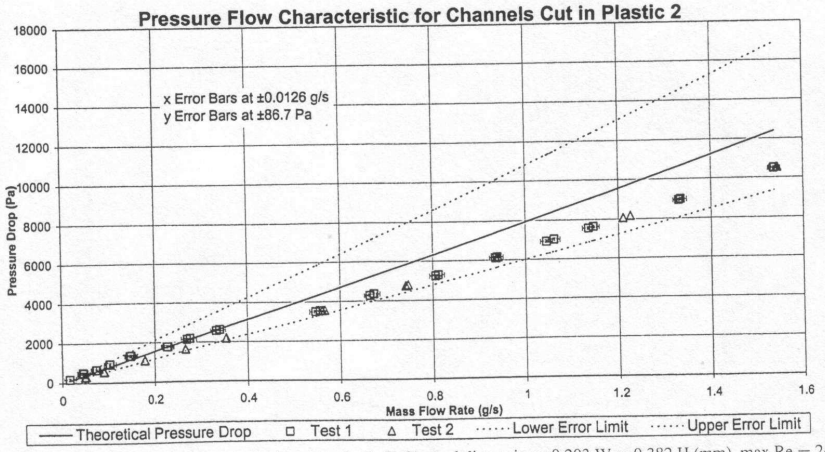

Figure 5 Pressure flow curve for channels cut in plastic 2. Channel dimensions: 0.203 W × 0.382 H (mm), max Re = 240.

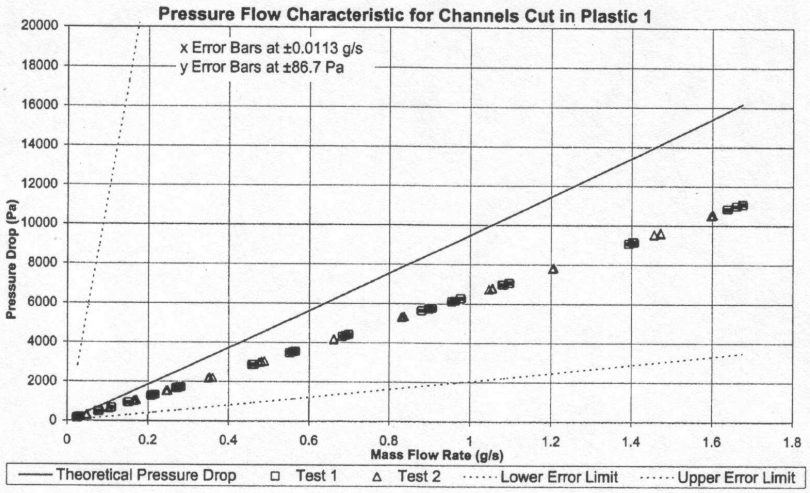

Figure 6 Pressure flow curve for channels cut in plastic 1. Channel dimensions: 0.202 W × 0.344 H (mm), max Re = 279.

DRIE and diced silicon channels fall within the error envelope. The pressure flow curves also show that the pressure and flow rate relationship is almost perfectly linear. This result is exactly as expected for laminar flow. The slight non-linearity is because of the entrance and exit effects discussed in the Calculations section.

Part 1 of this paper measures the channels in two ways. The first takes a single vertical and horizontal measurement from each channel, calculates the area of each channel idealized as a rectangle or trapezoid, and averages these areas to give an average area for the sample. The second method measures points taken from a SEM photograph of the channel and uses them to build an accurate CAD model of the real channel cross section. The change in the cross-sectional area data is copied from Part 1 of this paper [1] to Table 5.

The theoretical pressure flow characteristic curve is calculated using a Matlab program treating the channels as perfect rectangles or trapezoids. The error envelope shown with the dashed lines on each side of the theoretical line is found by recalculating the pressure drop for the channels using the minimum and maximum channel sizes as found by adding or subtracting two standard deviations from the mean value. Statistically, this gives a 95% probability that all experimental results will fall within this envelope. The error bars on specific points on the graph also show the 95% confidence interval for that particular measurement.

To compensate for the fact that the channels are not perfect rectangles or trapezoids, the actual area of the channels was measured from digitized SEM photographs using the technique described in Part 1 of this paper [1].

By substituting the relations $D_h^2 \propto A$ and $u \propto A$ into Darcy's Equation for laminar flow where $f \propto 1/\mathrm{Re}$, the relationship between the theoretical pressure drop, the area compensated pressure drop, and the theoretical and measured cross-sectional areas are as shown in Eq. (4):

$$\frac{P_{L1}}{P_{L2}} = \frac{A_2^2}{A_1^2} \tag{4}$$

Applying this correction to the theoretical calculations improves the correlation between the theoretical wet etched and DRIE channel pressure drops and the experimentally measured pressure drops. The recalculated theoretical curves for the DRIE and wet etched channels are shown in the area-compensated curves in Figures 8 and 9.

Table 4 Scanning Electron Microscope (SEM) measurements of five sets of microchannels (95% confidence interval [CI] = average value ± 2× sample standard deviation)

	Wet etch	Diced silicon	DRIE	Plastic 1	Plastic 2
SEM data (measured/available)	22/22	20/61	22/22	22/22	22/22
Average CSA (mm^2)	0.1263	0.0218	0.1008	0.0728	0.0777
Standard deviation (mm^2)	0.00525	0.00223	0.00152	0.01791	0.01040
% Deviation (95% CI)	8.31%	20.47%	3.01%	49.17%	26.78%

Table 5 Comparison between SEM measurement of individual channels and CAD model created from points taken from a SEM photograph of the same channel

	Wet etch	Diced silicon	DRIE	Plastic 1	Plastic 2
CSA from SEM (mm^2)	0.126878	0.021827	0.102701	0.077563	0.100015
CSA from CAD model (mm^2)	0.131198	0.019002	0.100054	0.075792	0.093405
% Change	+3.41%	−12.94%	−2.58%	−2.28%	−6.61%

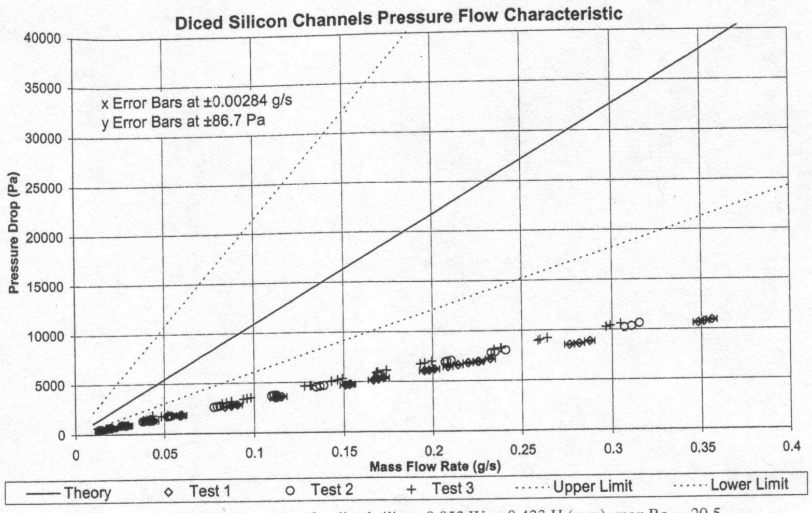

Figure 7 Pressure flow curve for diced silicon 0.052 W × 0.423 H (mm), max Re = 20.5.

This compensation does not improve the results from the other three channels. This means that some other, more significant effect must be causing the other, channels to deviate. For the plastic channels, the gap between the glass cover and the tops of the channels is the most likely cause of the experimental deviation. This is mostly filled by the SU8 photoresist used to bond the glass over the channels, but the slight warping in the plastic channels prevented a complete bond from forming. These are still within the uncertainty envelope calculated for them from theory, though they are likely to be better centered on the theoretical curve if the glass bond were complete.

The error in the diced silicon channels is most likely due to leakage occurring around the silicon sample in the test system. This is more likely to occur than with the other samples because the diced channels were not glass covered. Fluid leaking over the channels will increase the cross-section available for flow and, in doing so, give a far lower pressure drop for a given flow rate. The flow rates for the diced silicon channels are between a quarter and a tenth of the flows through the other channels, so the same amount of leakage over the channels will have a more significant effect on the results than it would have for the other channels tested.

The error in the DRIE channels is more difficult to explain. The DRIE channels are by far the most consistent in terms of their shape and size compared to any of the other channels tested. The results seem to indicate that the channels may

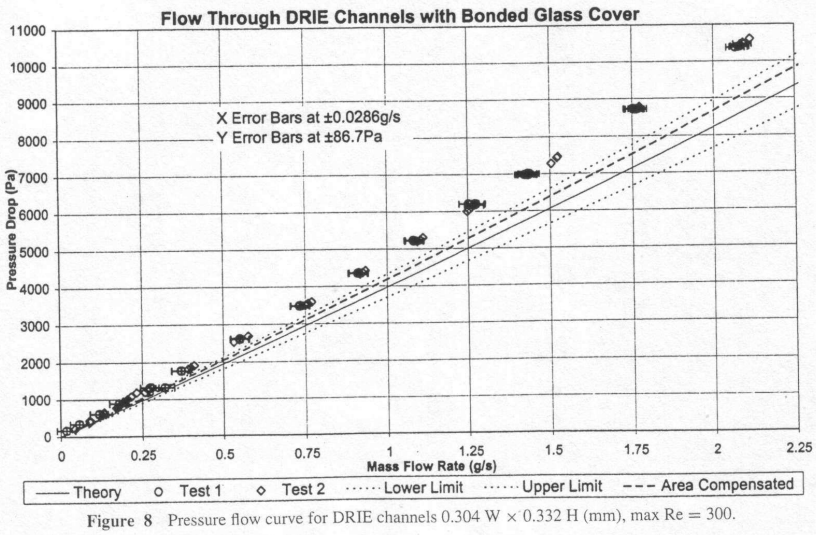

Figure 8 Pressure flow curve for DRIE channels 0.304 W × 0.332 H (mm), max Re = 300.

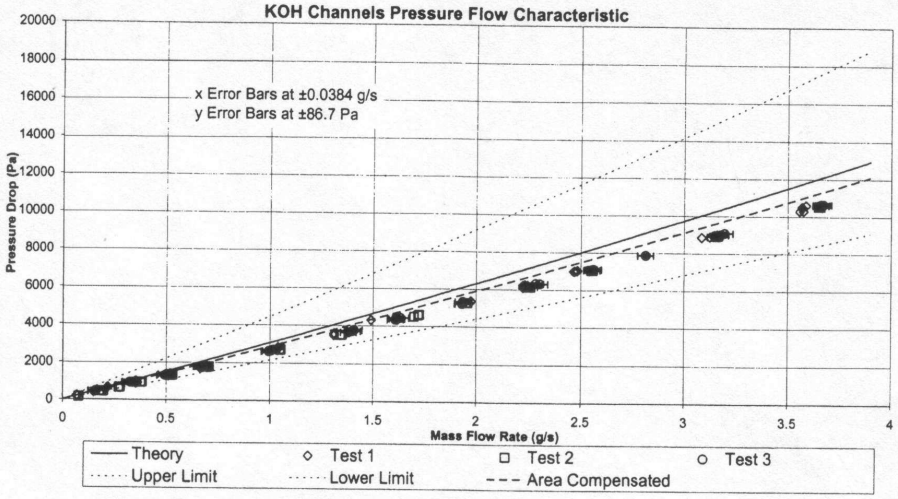

Figure 9 Pressure flow curve for wet etched channels 0.577 W × 0.413 H (mm), max Re = 417.

be smaller than the SEM data indicate. Since the cross-section is measured only at the plane of the entrance of the channel, there's a possibility that the channel cross-section changes further down the channels. Area compensation improves the theoretical results, just failing to bring the experimental pressure flow curve for the DRIE channels within the theoretical uncertainty envelope. Fully developed flow is assumed for theoretical calculations, so calculations, may need to be modified to account for developing flow.

In order to compare the results measured for these experiments with those measured by other researchers, the friction factor times Re, as measured from the experimental work, was divided by the theoretical $f\mathrm{Re}$ values calculated for each channel shape using similar data [6, 7]. Figure 10 is a plot of the normalized $f\mathrm{Re}$ measured from the experiments described here and elsewhere [4, 5]. The closer each y value is to one, the better it correlates with accepted macroscale flow theory.

A variety of triangular and trapezoidal microchannels are tested in [4]. Results from the wet etched channels tested in this paper correlate well with these results and are within 15% of theory. The N1-4000 channel has the closest hydraulic diameter to the wet etched channel tested here. Friction factors from channels 25 mm wide and of heights varying from 0.1 to 1 mm are measured in [5]. However, all of these have significantly higher aspect ratios than the rectangular channels tested. All of the rectangular channel data apart from that from

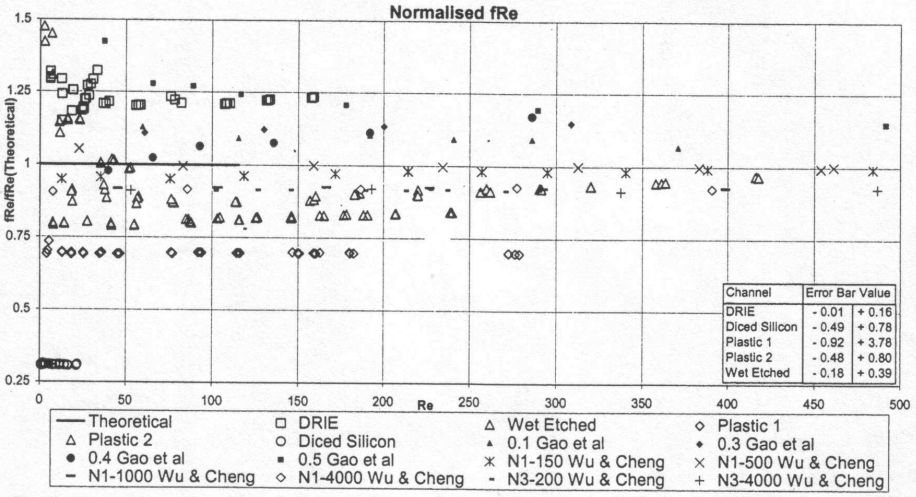

Figure 10 Normalized friction factor times Re for the channels tested compared with normalized data from other researchers.

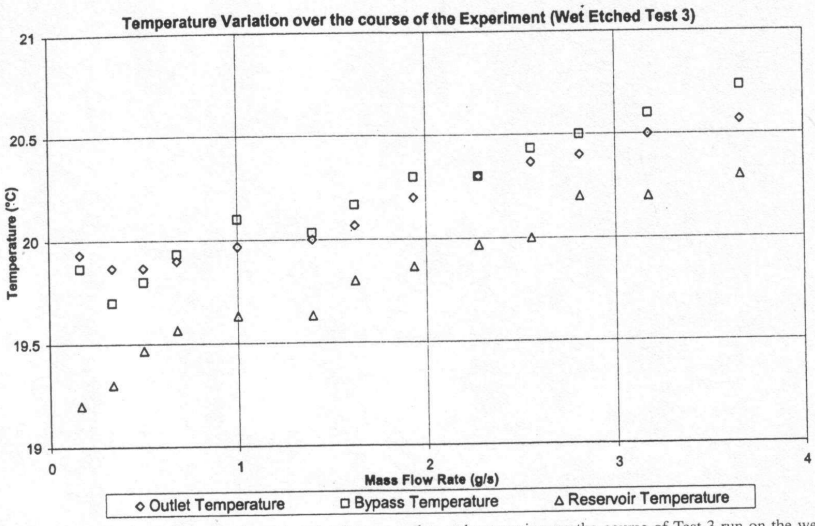

Figure 11 Temperature variation in the fluid in the channel outlet, bypass outlet, and reservoir over the course of Test 3 run on the wet etched (trapezoidal) channels. Room temperature was 19.6°C for this experiment.

the diced silicon channels correlate quite well with theoretical values.

Figure 11 shows a plot of the variation in the temperature of the fluid for Test 3 on the wet etched channels. All recorded temperatures were similar for each experiment. Temperature variation is almost entirely due to heating from the pump. This can be seen in the bypass fluid temperature, which is slightly higher than the temperature of the fluid that has passed through the channels. The bypass is closer to the pump than the outlet from the channels and therefore has less time to lose the heat to the ambient air.

The stepping in the temperature of the reservoir is due to the water collected for weighing being poured periodically back into the reservoir. The system is left to stabilize after this has been done in order to ensure that the increase in the height of the reservoir does not affect the system. Height changes are a maximum of 8 mm (7.8 Pa), so this change should not affect flow in the system significantly.

CONCLUSIONS

The general flow behavior correlates very well with standard macroscale laminar flow theory. The 95% confidence interval for the results perfectly encompasses three of the five channels tested.

The test on the diced silicon channels shows clear evidence of leakage over the channel sample. This will be improved in subsequent experiments by increasing the clamping pressure over the channels and using a more compliant gasket material.

The DRIE channel results are the only measurements that initially seem to deviate in an experimentally significant way from the theoretical calculations. However, when the flow curve is modified to compensate for the difference in area between the perfect rectangular channel assumed by the theoretical model and the actual cross-sectional area of the channel measured from the CAD model, the theoretical flow curve shifts far closer to the behavior measured during the experiment.

The fRe values calculated from the system correlate reasonably well with theory and work of other researchers. The 95% CI on these measurements indicates a high level of error in the calculation of the fRe values.

The heating effect of the pump is not enough to change the properties of the test fluid significantly over the course of an experiment. The microchannels tested here do not show experimentally significant differences in behavior compared to larger channels.

NOMENCLATURE

A	cross-sectional area of a channel, m^2
$A1$	cross-sectional area for contraction loss, m^2
$A2$	cross-sectional area for contraction loss, m^2
C	pressure transducer calibration constant, Pa/V
D_h	hydraulic diameter, m
f	friction factor
K_L	loss coefficient
L	length of channel, m
M	liquid mass flowing through system, g
$\dot{m}$	mass flow rate, g/s
n	pump RPM, rev/min
P_L	pressure drop along channel, Pa
Re	Reynolds number
t	time taken for fluid to be collected, s
T_{bp}	fluid temperature at bypass outlet, K

T_o fluid outlet temperature, K
T_{res} reservoir temperature, K
u mean velocity of fluid in test channel, m/s
V_{bp} bypass valve setting, rev
V_m master valve setting, rev
V_P pressure transducer voltage, V
w_m uncertainty in mass measurement, g
$w_{\dot{m}}$ uncertainty in mass flow, g/s
w_t uncertainty in time measurement, g/s

Greek Symbols

μ viscosity of fluid, Pa s
ρ density of fluid, kg/m^3

REFERENCES

[1] Eason, C., Dalton, T., O'Mathúna, C., Slattery, O., and Davies, M., Direct Comparison between Five Different Microchannels, Part 1: Channel Manufacture and Measurement, *Heat Transfer Engineering Journal*, vol. 26, no. 3, pp. 00–00, 2005.

[2] Paputski, I., Gale, B. K., Mohanty, S., Ameel, T. A., and Frazier, A. B., Effects of Rectangular Microchannel Aspect Ratio on Laminar Friction Constant, *Proc. SPIE—The International Society for Optical Engineering, Proc. 1999 Microfluidic Devices and Systems II*, Santa Clara, vol. 3877, pp. 147–158, 1999.

[3] Judy, J., Maynes, D., and Webb, B. W., Characterization of Frictional Pressure Drop for Liquid Flows through Microchannels, *International Journal of Heat and Mass Transfer*, vol. 45, pp. 3477–3489, 2002.

[4] Wu, H. Y., and Cheng, P., Friction Factors in Smooth Trapezoidal Silicon Microchannels with Different Aspect Ratios, *International Journal of Heat and Mass Transfer*, vol. 46, pp. 2519–2525, 2003.

[5] Gao, P., Le Person, S., and Favre-Marinet, M., Scale Effects on Hydrodynamics and Heat Transfer in Two-Dimensional Mini and Microchannels, *International Journal of Thermal Sciences*, vol. 41, pp. 1017–1027, 2002.

[6] Çengel, Y. A., *Heat Transfer, a Practical Approach*, p. 380, Boston, MA: McGraw Hill, 1998.

[7] Rohsenow, W. M., Hartnett, J. P., and Ganic, E. N., *Handbook of Heat Transfer Fundamentals*, 2nd ed., pp. 7–91, 7–118, New York, USA: McGraw Hill, 1985.

[8] Howatson, A. M., Lund, P. G., and Todd, J. D., *Engineering Tables and Data*, 2nd ed., London, England: Chapman and Hall, 1995.

[9] Holman, J. P., and Gajda Jr., W. J., *Experimental Methods for Engineers*, 5th ed., pp. 41–42, New York, USA: McGraw Hill, 1989.

Cormac Eason graduated from the University of Limerick in 2001 with a first class honours B.Eng. degree in mechanical engineering. He has since worked in the Stokes Research Institute toward his PhD. His current research area is in microchannels.

Tara Dalton is currently the manager of the Stokes Research Institute. She has a B.Eng. in Aeronautical Engineering, awarded in 1994, and her Ph.D., awarded from the University of Limerick in 1997, is on enclosure heat transfer as applied to electronic reliability design. At present, she is engaged in managing the research contracts awarded to the Centre, augmenting the research funding for the Centre, supervising postgraduate students, and lecturing internationally on electronic thermal design and reliability. Her current research interests primarily include electronic reliability, development of fundamental measurement methods, and dimensional analysis in heat transfer and fluid mechanics.

Mark Davies is a Professor of Engineering Science and Director of Stokes Research Institute (www.stokes.ie) at the University of Limerick. His B.Sc. is in Mechanical Engineering from the University of Bath, and his Ph.D. is in Aeronautical Engineering from the University of Cambridge. His interests have ranged over many problems in thermofluidics; presently, he is focused on developing microfluidic systems for cancer diagnostics.

Seán Cian O'Mathúna received his B.E., M.Eng.Sc., and Ph.D. degrees from the National University of Ireland, Cork, in 1981, 1984, and 1994, respectively. From 1982 to 1993, he was Co-Manager of the Interconnection and Packaging Group, National Microelectronics Research Centre (NMRC), University College Cork, Ireland. In 1993, he joined PEI Technologies, NMRC, as Technical/Commercial Director, where he was responsible for power packaging, planar/integrated magnetics, and product qualification. In 1997, he rejoined NMRC as Group Director, with a responsibility for microsystems. In 1999, he was appointed Assistant Director for NMRC, with a responsibility for microelectronics integration with research themes in ambient electronics, biomedical microsystems, and energy processing for ICT. He is co-author of more than 25 journals papers, 60 conference papers, and two book chapters.

Orla Slattery obtained a B.E. in civil engineering from the University College Cork in 1989, an M.Eng.Sc. (civil engineering) degree in 1991, and an M.Eng.Sc. (electronics) degree in 1998. In 1991, she joined the Interconnection and Packaging Group at NMRC, where she was responsible for the simulation and characterization of thermal and thermomechanical issues in electronics components and systems. Since 1999, she has been working as a research scientist with the Computational Modelling Group in NMRC. She has participated in a number of European Union- and Irish Government-funded projects as well as provided services to the Irish and European industry. Her current research interests include the application of computational simulation tools to the solution of thermal and thermomechanical problems in microelectronics components and systems. She has published a range of papers in these areas. She is also involved in the modeling and simulation of MEMS and is currently the vice-chair of the EU-funded Network of Excellence on Design for Micro and Nano manufacture, PATENT-DfMM.